Available online at www.sciencedirect.com
ScienceDirect
Journal of the European Ceramic Society 27 (2007) 2705–2713
www.elsevier.com/locate/jeurceramsoc

High temperature water vapour corrosion of rare earth disilicates $(Y,Yb,Lu)_2Si_2O_7$ in the presence of $Al(OH)_3$ impurities

N. Maier [a,1], K.G. Nickel [a,*], G. Rixecker [b,1]

[a] *Eberhard-Karls-University Tuebingen, Applied Mineralogy, Wilhelmstr. 56, D-72074 Tuebingen, Germany*
[b] *Max-Planck-Institute for Metals Research, Heisenbergstr. 3, D-70569 Stuttgart, Germany*

Received 12 June 2006; received in revised form 21 September 2006; accepted 24 September 2006
Available online 15 November 2006

Abstract

Potential environmental barrier silicates based on rare earth disilicates containing Y, Yb and Lu have been investigated for their corrosive behavior in a gas stream containing water at 1500 °C. No currently used test method is unambiguous: silica or silica-forming tubing cause high internal $P_{Si(OH)_4}$, which should artificially slow down corrosion rates and alumina tubing cause alumina contamination via $P_{Al(OH)_3}$. We used the latter and report on the details of the interaction. In $Y_2Si_2O_7$ and a number of solid solutions with a Lu or Yb content up to 50% this contamination resulted in the formation of a melt. Depending on further impurities, particularly Ca, melt formation is accompanied by oxyapatite or monosilicate crystallisation. On cooling rare earth garnets crystallize from the melt. The melt ± oxyapatite/monosilicate formation does not create a protective effect. The corrosion kinetics is linear; the rates are slower than those of pure silica, but only at a level reflecting reduced silica activity due to dilution by a factor of 2–5. Porosity causes fast initial mass losses. The formation of secondary phases inside the material induces crack formation. A disilicate layer in those systems is unlikely to become an effective environmental barrier for non-oxide systems.

For Yb and Lu silicates there are indications for the formation of a rare earth garnet layer during the corrosion process at high temperature, which has protective power. This causes a logarithmic law for the corrosion kinetics: for extended times the mass loss drops asymptotically. Under the assumption that the garnet formation also removes the sink for external alumina, the protection for Si-removal may even become perfect. The total mass change is a balance between Al-input and silica loss, which makes it currently impossible to formulate a quantitative equation for the time dependence of the process.

Keywords: Corrosion; Impurities; Environmental barrier coating; Silicate; SiO_2

1. Introduction

For next generation gas turbines with high efficiency and low emission, there is a need for new materials to replace the currently used Ni based alloys in order to allow higher combustion temperatures.[3,4] SiC and Si_3N_4 are potential materials for the use in turbine environments as they show excellent high temperature strength and durability.[3,6,7] Unfortunately, the corrosion resistance of these materials in combustion environments, which contain considerable amounts of water vapour,[8] is relatively poor. In such environments, a protective silica scale formed on top of silicon carbide or nitride is constantly removed by a reaction of silica with H_2O:

$$SiO_2 + 2H_2O(g) \rightarrow Si(OH)_4(g) \quad (1)$$

Fast gas flow rates cause a fast removal of $Si(OH)_4$ from the material surface and thus a fast degradation of the SiC or Si_3N_4, making these ceramics unsuitable for the use in turbine environments without additional protective measures[9–11] such as coatings. Among the candidates for environmental barrier coatings ("EBC") are rare earth disilicates, $RE_2Si_2O_7$ (RE = rare earth element, including Y and Sc). These silicates can also form a volatile silicon hydroxide by a reaction

$$RE_2Si_2O_7 + 2H_2O \rightarrow RE_2SiO_5 + Si(OH)_4(g), \quad (2)$$

leaving a porous surface scale of monosilicates RE_2SiO_5.[4,12] The rate of material loss was found to be slower than for silica

* Corresponding author. Tel.: +49 7071 297 6802; fax: +49 7071 293060.
E-mail address: klaus.nickel@uni-tuebingen.de (K.G. Nickel).
[1] Present address: Robert Bosch GmbH, CR, Postfach 10 60 50, D-70049 Stuttgart, Germany.

0955-2219/$ – see front matter © 2006 Elsevier Ltd. All rights reserved.
doi:10.1016/j.jeurceramsoc.2006.09.013

scales on SiC or Si_3N_4. Some experimental results[4] indicate that the monosilicate could become protective for the $RE_2Si_2O_7$ underneath. Even though monosilicates show a higher stability in wet atmospheres, disilicates remain attractive EBC materials because of

- a low thermal expansion coefficient mismatch compared to Si_3N_4 or SiC[7,13] and
- the native oxidative formation of $RE_2Si_2O_7$ on Si_3N_4 or SiC containing rare earth sintering additives.[14,15] The poor results of previous experiments on silicate formers[10] may not be valid for all sample compositions.

Up to now, data on the hydro corrosion behaviour of rare earth disilicates are scarce and sometimes contradictory.[3,4,16–19] Therefore our studies aimed for a better understanding of the corrosion mechanisms of these materials in hot and wet atmospheres. It was also intended to check the reported better hydro corrosion resistance of disilicates containing rare earth elements with small ionic radii[20] and whether solid solutions of different $RE_2Si_2O_7$ compounds have different corrosion resistance.

Unfortunately, the contamination of our samples with aluminium during corrosion had a strong influence on the corrosion behaviour of the materials, so these original questions could not be solved unambiguously. Instead, new and important insights in the corrosion mechanisms in the presence of Al could be gained, which are of relevance for practical applications and further experimental work and which allow a better understanding of literature reports on the hydro corrosion of $RE_2Si_2O_7$ and the contradictions found therein.

Recent studies on the hydro corrosion behaviour of rare earth disilicates concentrated on materials, which do not show polymorphism (Yb or Lu disilicates), because a volume change during phase transformation was envisaged to be disadvantageous for the stability of an EBC.[3] However, in previous studies we found the γ polymorph of $Y_2Si_2O_7$ to be stable between approximately 1320 °C and ≥1600 °C with a sluggish transformation kinetics down to 1200 °C.[21,22] Thus this material could behave well in real applications. Furthermore, at least the solid solution materials with $Y \leq 50$ mol% + Yb or Lu are not expected to show any polymorphism in a temperature range between <1000 °C and approx. 1600 °C[22] and might thus be promising candidates for EBCs.

2. Experiments

From attrition milled and cold isostatically pressed mixtures of oxide powders we synthesised samples by reaction sintering. The oxide powders used were SiO_2 (CERAC, 99.9% purity), Y_2O_3 (H. C. STARCK, 99.9% purity), Yb_2O_3 (CHEMPUR, 99.99% purity) and Lu_2O_3 (ABCR, 99.9% purity). Sintering runs were conducted at temperatures between 1400 °C and 1600 °C in NABERTHERM chamber kilns. Samples were contained in covered platinum crucibles during sintering. The sintered samples with the abbreviations used in this paper are listed in Table 1.

Table 1
Sample compositions and labelling

Label	Powder mixture (molar ratios)	Sinter product
Lu	2 SiO_2:1 Lu_2O_3	$Lu_2Si_2O_7$
Yb	2 SiO_2:1 Yb_2O_3	$Yb_2Si_2O_7$
50YLu	2 SiO_2:0.5 Lu_2O_3:0.5 Y_2O_3	$(Y_{0.5}Lu_{0.5})_2Si_2O_7$
50YYb	2 SiO_2:0.5 Yb_2O_3:0.5 Y_2O_3	$(Y_{0.5}Yb_{0.5})_2Si_2O_7$
75YLu	2 SiO_2:0.25 Lu_2O_3:0.75 Y_2O_3	$(Y_{0.75}Lu_{0.25})_2Si_2O_7$
75YYb	2 SiO_2:0.25 Yb_2O_3:0.75 Y_2O_3	$(Y_{0.75}Yb_{0.25})_2Si_2O_7$
Y	2 SiO_2:1 Y_2O_3	$Y_2Si_2O_7$

After the treatment only fractions below 1% of monosilicates RE_2SiO_5 were found and thus a similarly small amount of silica rich phase can be expected in a disilicate matrix, indicating nearly complete reaction. In the range of the compositions of this study complete solid solubility was observed.[22]

Sintering densities of most samples were >95% of the theoretical values (approximating the theoretical densities of the solid solutions as mean values of the end member densities). Only the samples 75YYb and Y showed poor densification with approximately 88% and 70% theoretical density, respectively. For further details, see Refs. 21,22.

In corrosion experiments, cut and polished samples of the sintered disilicates with surface areas of approximately 3 cm^2 were placed on a U-shaped platinum holder. The succession of the samples was according to Table 1 (Lu in front, Y at the end). Given the alleged lower volatility of $RE_2Si_2O_7$ containing smaller rare earth element ions,[3,20] this sample order should help minimising saturation effects in the corroding gas phase.

The sample holder was placed in the alumina furnace tube of a XERION Xtube 1700 furnace, which was pre-aged to remove alkalis, as shown schematically in Fig. 1. The furnace was heated to 1500 °C in several steps: 2 °C/min to 100 °C, 4 °C/min to 300 °C, 8 °C/min to 1300 °C, and 6 °C/min up to

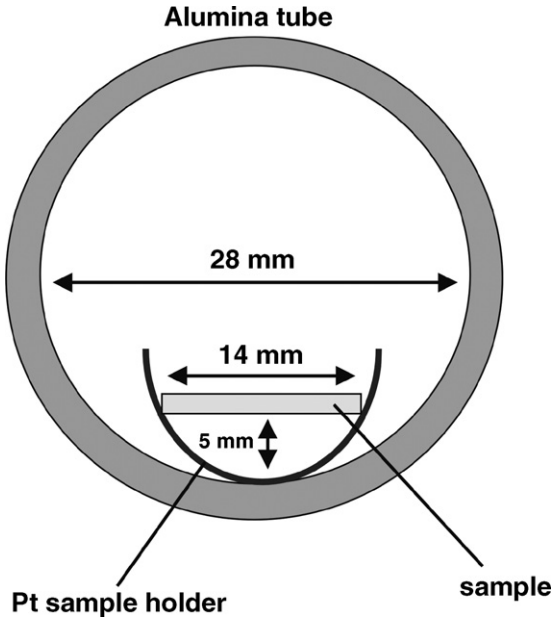

Fig. 1. Schematic sketch of the sample positioning in the furnace tube.

Table 2
Mass loss in mg cm^{-2}

Time (h)	Lu	Yb	Y	SiO_2	50YLu	50YYb	75YLu	75YYb
20	0.067	0.124	0.176	0.187	0.080	0.075	0.059	0.047
50	0.063	0.184	0.190	0.335	0.107	0.093	0.073	0.051
120	0.088	0.263	0.227	0.869	0.164	0.170	0.139	0.094
310	0.078	0.308	0.449	1.923	0.301	0.346	0.243	0.251

1500 °C. A gas flow of ≈290 l/h was switched on after reaching the plateau temperature. This resulted in a calculated gas flow velocity at room temperature[23] of approximately 13 cm/s in the furnace tube. After the treatment a cooling rate of 5 °C/min was chosen.

The gas consisted of 70 vol.% air and 30 vol.% water vapour (P_{H_2O} = 0.3 bar at 0.1 MPa total pressure). To obtain a constant gas flow with constant water vapour content, a modified version of a set-up used by Opila[24] was used, in which a glass bead filled washer flask at 70 °C was used as the condensation unit for a bubbler unit at 75 °C. Measurements of the gas exit confirmed a water vapour content of about 95% of the calculated saturation value.

Temperature profiles of the furnace with activated gas flow were recorded before the start of the corrosion tests to make sure that all samples were indeed placed in positions with T = 1500 °C during corrosion experiments. Temperature measurements at different sample positions during the experiments never showed deviations of more than 3 °C from the designated corrosion temperature.

Mass losses of the corroded materials were evaluated by measuring the weight of the samples before and after corrosion runs for 20, 50, 120 and 310 h. Scanning electron microscopy and EDX analysis (ZEISS DSM982 Gemini, DSM 962 and LEO 438-38-06) examinations were conducted with as-corroded samples and a number of polished cross-sections to gather information on phase content and distribution after corrosion. Supporting surface XRD measurements on corroded samples were made using a PHILLIPS PW1050 diffractometer with Cu Kα radiation to study the crystalline phase content.

3. Results

The measured mass losses relative to the sample surface (≈3 cm^2) after different corrosion treatments are given in Table 2. The data given are raw data as measured and need to be interpreted in the light of the results outlined below. Nonetheless it is clear from Table 2 that all samples lost mass during the treatment and that the loss from pure silica is much higher then the loss from silicates.

The data interpretation is not meaningful unless the development of the microstructure is taken into account. All disilicate samples show crystals of newly-formed rare earth aluminium garnet $RE_3Al_5O_{12}$ on their surfaces (Fig. 2) along with a clearly visible grain boundary attack in the disilicate. Fig. 2 shows only 50YYb samples but the features are typical for all experiments.

The existence of garnet phase is evidence for the contamination of the samples with aluminium during corrosion. The aluminium is most probably carried from the furnace tube to the sample surfaces via gas phase transport of volatile $Al(OH)_3$ formed by a reaction of the alumina with water vapour.[3,25]

Upon longer exposure, the garnet covers increasing portions of the upper surface of the samples. Monosilicate RE_2SiO_5 develops in addition. In Y-bearing systems, oxyapatite $RE_{9.33}(SiO_4)_3O_2$ is observed instead (sample Y) or in addition (samples 50YYb, 75YLu, 75YYb) as shown in Fig. 2b and c. The apatite incorporates several atomic% of calcium as measured by EDX. Calcium was most probably introduced as an impurity from the oxide powders and is mobilized during corrosion as described by.[26,27] It probably stabilises the apatite phase, which is not stable in pure Al_2O_3–SiO_2–RE_2O_3-Systems for RE = Y, Yb or Lu.[28] Higher contents of the apatite phase in corroded silicates with larger (mean) rare earth ionic radii and its absence in small rare earth disilicates Lu, Yb and 50YLu[22] is attributed to different Ca concentrations necessary for the stabilization of the phase. EDX measurements indeed show a decrease in Ca content in the newly-formed apatite phase from approximately 4 at.% in 50YYb to less than 3 at.% in sample Y.

The lower faces, pointing towards the sample holder during the experiments, differ from the upper faces. Only small amounts of newly-formed garnet and sometimes additionally sporadic monosilicate or apatite crystals are observed and there is no significant increase in coverage by garnet from the initial stage at 20–310 h (Fig. 2d and e). This is taken as evidence that the lower surfaces do not effectively take part in the corrosion process, because neither the contamination product garnet nor the corrosion product monosilicate covers large areas. We attribute this to poor flow conditions beneath the row of samples as discussed elsewhere.[21] The phenomenon has to be taken into account in the calculation of corrosion rates: the values in Table 2 must be multiplied by a factor of 2 to get approximate values for the effective mass loss rates.

An exception is the Lu sample, which is the first sample in the holder. Here a graded phase distribution after 310 h exists with a garnet rich lower surface passing over into disilicate coexisting with monosilicate towards the back end of the sample. For details see Ref. 21.

Fig. 3a shows a cross section from a corrosion test with 50YYb for 310 h. This figure, which is typical for most Y-bearing dense samples, illustrates that (a) garnet formation is surficial and only rarely found at deeper levels, (b) the surface layer tends to obscure monosilicate below, (c) monosilicate is occurring also at greater depths, and (d) monosilicate is not intimately associated with garnet.

The cross section of the Yb-material (Fig. 3b) is somewhat different because here, the monosilicate is almost entirely in con-

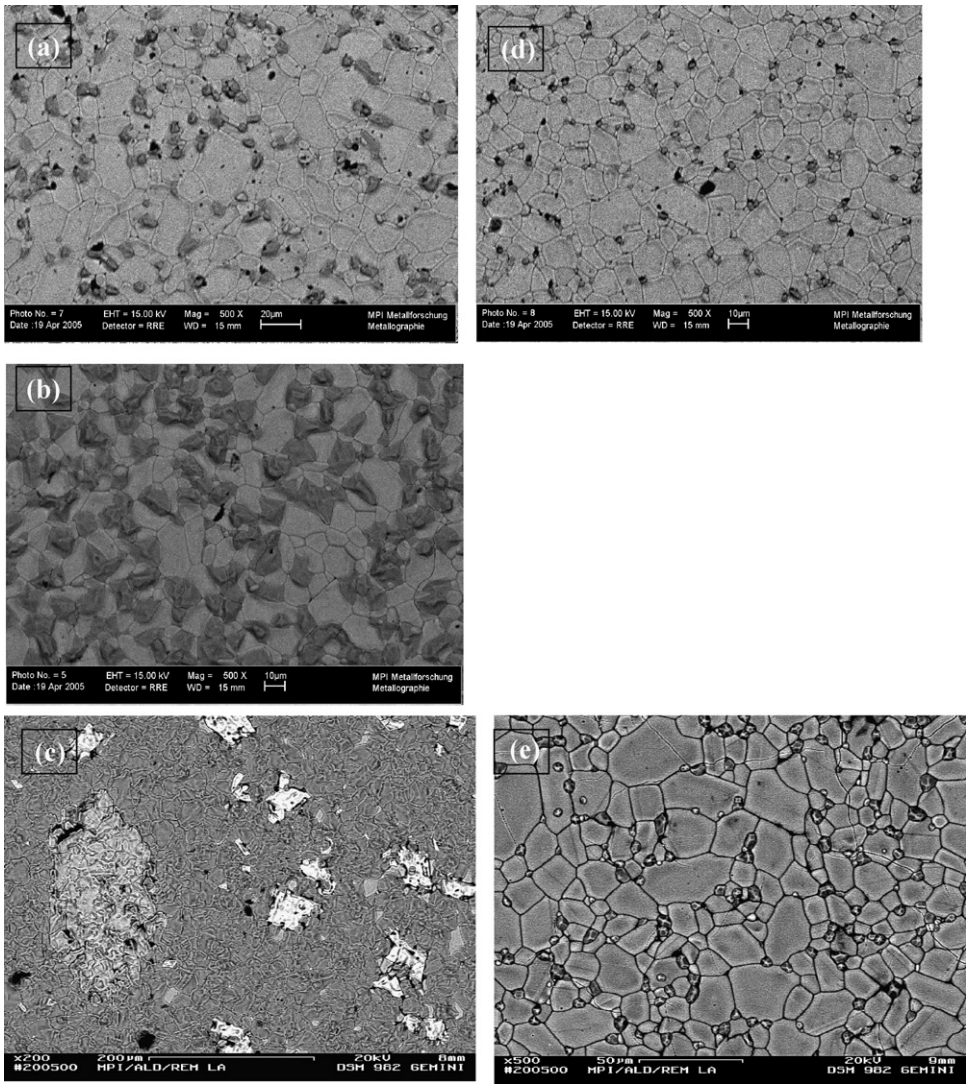

Fig. 2. SEM Surface views of 50YYb after corrosion; light grey: disilicate; dark grey: garnet, black: pores; medium light grey in (e): apatite. Upper surface after 20 h (a), 120 h (b), 310 h (c), lower surface after 20 h (d) and 310 h (e).

tact with the surficial garnet. This stratification was also observed in the pure Lu-material.

Another case is the very porous $Y_2Si_2O_7$ "Y"-material, which shows corrosive attack even far below the surface ($\gg$100 μm) without a well developed stratification in garnet-rich surface area and garnet-free, silica depleted subsurface zone (Fig. 4).

The numerous cracks present in the bulk of the samples (Figs. 3 and 4) seem to be associated with prolonged exposure times.

4. Discussion

All $RE_2Si_2O_7$ samples clearly show lower weight loss rates than silica (Table 1). The mass loss kinetics, taking into account the effective exposed area, is plotted in Fig. 5.

All Y-bearing samples (Fig. 5a) are reasonably described by simple linear corrosion kinetics. However, the fits do not go through the origin and hence the significant off-sets need to be explained. The samples with pure Lu- and Yb-disilicates (Fig. 5b) are approximated by a simple asymptotic behaviour (logarithmic law[29]).

As shown above, there is Al intake for all samples. Therefore, the loss rates are not identical to those true for a simple system according to the disilicate to monosilicate reaction (Eq. (2)), but lowered by counterbalancing impurity ingress.

The linearity of the process in Fig. 5a suggests that the formation of surficial garnet is not creating a barrier for the evaporation of $Si(OH)_4$ and the similarity in slope indicates similar corrosion velocities: samples with even up to 50 mol% Lu or Yb do not seem to give any significantly better protection than pure or high-Y disilicates.

Saturation effects in the gas phase (increasing $Si(OH)_4$ content and decreasing $Al(OH)_3$ content in downstream direction) may have some influence on the measured mass loss rates[21] and this might obscure minor differences in loss rates of different Y-Yb/Lu mixtures.

On the other hand, pure Yb and Lu samples seem to follow a law, which represents decreasing mass loss with time (Fig. 5b).

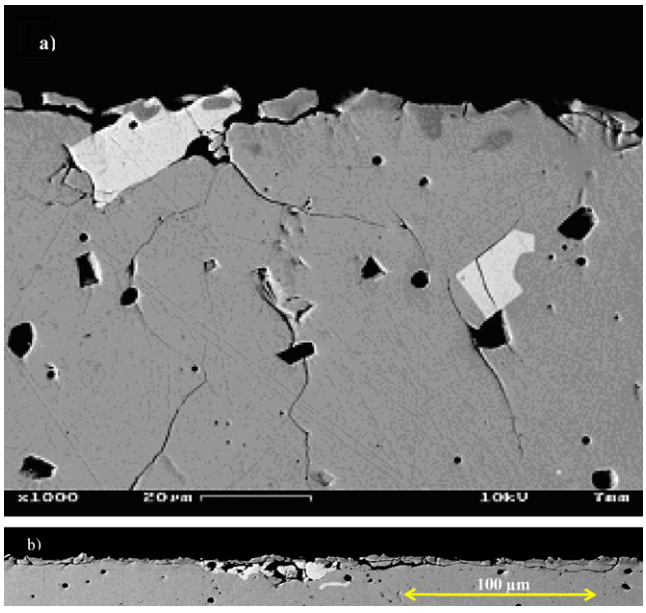

Fig. 3. SEM of cross section of (a) 50YYb and (b) Yb after 310 h. The dark grey phase is garnet, light phase is monosilicate, black: pores, remainder is disilicate.

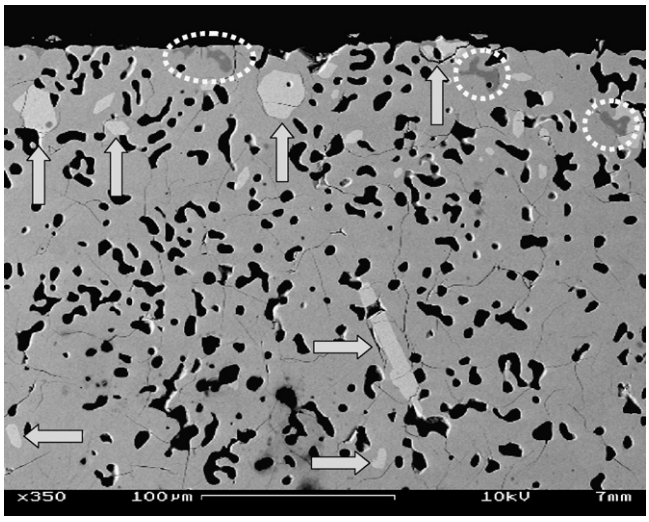

Fig. 4. REM cross section of upper face of $Y_2Si_2O_7$ "Y"-material after 310 h; arrows mark apatite, circles mark garnet.

Thus in this case a protective effect by garnet formation seems likely.

The appearance of phases is best discussed using the relevant phase diagrams. Currently available are two versions of the liquidus surface of the system Y_2O_3–Al_2O_3–SiO_2[1,2] and an isothermal section at 1550 °C for the system Yb_2O_3–Al_2O_3–SiO_2.[5] Dr. Olga Fabrichnaya kindly provided us with a calculated isothermal section at 1500 °C of the Y-system based on her data set.[2] The isothermal sections based on those references are shown in Fig. 6.

In Fig. 6 it is shown that all three diagrams predict a different phase assemblage to become stable with an alumina uptake modifying the composition of the pure disilicate. The diagram of Bondar[1] predicts a silica-rich melt along with the oxyapatite $Y_{9.33}(SiO_4)_3O_2$ (Y2S3 in Fig. 6a) to be stable with the disilicate $Y_2Si_2O_7$ (YS2 in Fig. 6), while the section based on[2] would predict a two-phase assemblage of a less silica-rich melt and disilicate to become stable. The Yb-system according to[5] would predict the rare-earth garnet $Yb_3Al_5O_{12}$ (A5Y3 in Fig. 6) to become stable together with a silicate melt and disilicate.

The problems with impurities, particularly Ca in rare earth oxide powders, have been discussed above. Therefore all three diagrams may reflect a true situation: Fig. 6a for the impurity laden system, Fig. 6b for the Y- (Y/Yb-, Y/Lu-) system with Ca concentrations too small for the stabilisation of oxyapatite and Fig. 6c for the Yb- and possibly the Lu-system, because the ionic radius of Lu^{3+} is very similar to Yb^{3+}. Fig. 6c is for 1550 °C, hence at 1500 °C the liquid field should be smaller and contracted towards more silica-rich compositions.

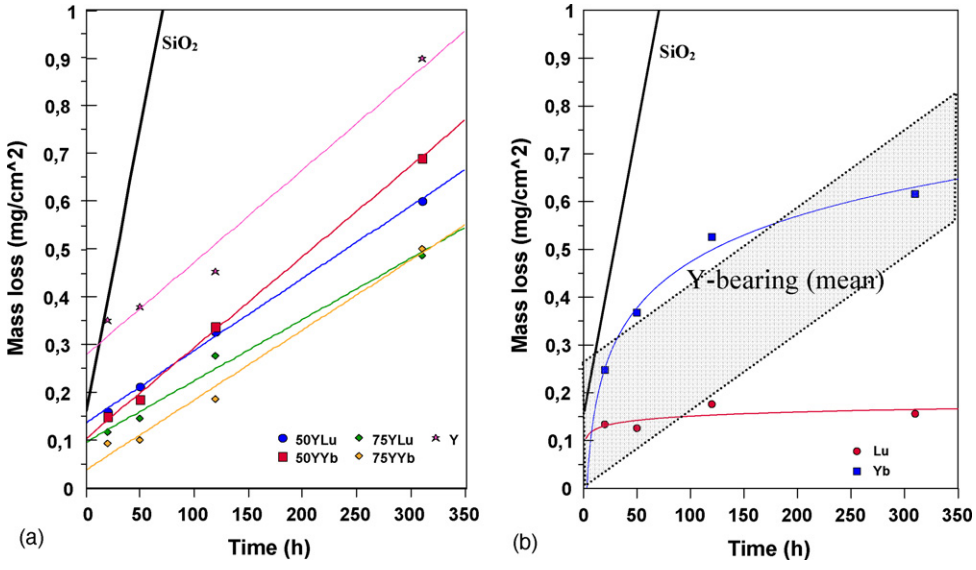

Fig. 5. Recalculated mass losses of disilicates as a function of time: (a) Y-bearing samples and (b) pure Lu and Yb-samples in comparison to the silica reference sample.

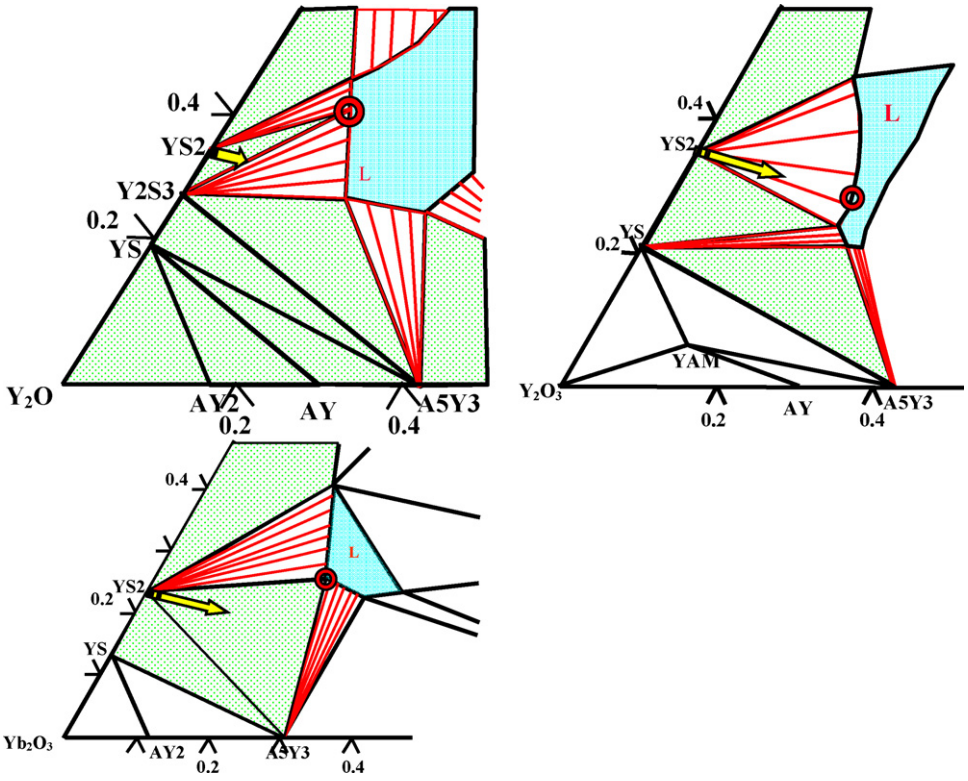

Fig. 6. Isothermal sections (wt%) at 1500 °C for Y_2O_3–Al_2O_3–SiO_2 based on (a),[1] (b)[2] and (c) an isothermal section at 1550 °C for the system Yb_2O_3–Al_2O_3–SiO_2.[5] The hatched areas mark three-phase assemblages of interest. The arrows indicate the concentration change caused by alumina uptake, the rings indicate the melt composition predicted to become stabilized.

Fig. 6a would predict a phase assemblage of disilicate, oxyapatite and a fairly silica-rich melt to become stable at 1500 °C both for Al uptake and for straight silica loss from disilicate. Fig. 4 shows indeed a significant amount of oxyapatite near the surface but also inside the sample.

Due to the porous nature of the original Y sample it has a large surface exposed to the atmosphere in the beginning. This could explain the high initial loss found in Fig. 5. The large size and isolated occurrence of crystals of oxyapatite suggests a strong sintering, respectively recrystallisation. The melt formed during corrosion could have helped in the process and may also have clogged the porosity near the surface, which is not uncommon for silica melts on porous substrates.[30,31] This would cause a kinetic break, because after pore closure the surface exposed is identical to the geometric surface.

At this stage no garnet should form and in Fig. 6a there is no equilibrium between disilicate and garnet. Not even the room temperature equilibria, which can be deduced from,[1] would allow such an assemblage because disilicate with some alumina uptake would crystallize to disilicate + oxyapatite + mullite, and a silica depleted composition should yield monosilicate + oxyapatite + garnet. Neither of both is observed.

Bearing in mind that apatite formation is related to Ca-impurities the situation can be discussed based on Fig. 6b. It would predict a binary assemblage of melt and disilicate at high temperature for an Al-enriched composition. A silica depleted composition would have disilicate + monosilicate + liquid as an equilibrium assemblage. Only on cooling to room temperature one would find an equilibrium between disilicate, monosilicate and garnet.

Our observed phase assemblage is disilicate + oxyapatite + garnet. Hence the truth seems to lie in-between the two scenarios: At first we have the high temperature formation of apatite and liquid. Ca becomes concentrated in the apatite and so during cooling the system behaves as a pure one, yielding garnet. Additional monosilicate could appear at this stage. The round shape of garnets in Fig. 4 makes an origin from a crystallizing melt likely.

Therefore the pure Y-system changes after an initial fast corrosion stage on the large surface into a system, which loses its silica via the melt formed from the Al-input and at most only partly directly from disilicate. This situation does not change much with time and consequently linear kinetics prevails during the observed time.

The Y-free Lu- and Yb-systems behave differently. The isothermal section (Fig. 6c) predicts, at least for the Yb-system, a direct conversion into an assemblage disilicate + garnet + melt on Al uptake. Depending on the amount of concurrent silica loss we would either find this assemblage stable at high temperature, or the binary disilicate + garnet or the disilicate + monosilicate + garnet assemblage.

In Fig. 3b an association of monosilicate with garnet is visible. However, the garnet covering the surface is not always connected to monosilicate. A model for a stratification of this type would involve the Al-incorporation to produce surficial garnet and melt at temperature. The silica loss has to occur through

the silica melt, which would cause more disilicate to disproportionate at the bottom. This process may be controlled by nucleation problems, which explains the local appearance of the monosilicate phase. Furthermore, some of the monosilicate could also originate during cooling.

The garnet is silica free and will not take part in the silica loss. It is also not likely to loose alumina, because the atmosphere contains $Al(OH)_3$ and is hence saturated in Al. Garnet is a stoichiometric phase and hence does not act as a sink for further Al. Therefore the garnet can become protective. If it has zero loss than the logarithmic law of kinetics is a physically sensible kinetic law.

The difference in kinetics of the Yb and Lu systems (Fig. 5b) would then come primarily from a different velocity of coverage by garnet. There are, however, a number of uncertainties with the Lu material. Firstly, the sample was the first in the gas stream and hence it may have depleted the gas in Al for the next sample, the Yb material. However, the following samples, including the silica sample at the end of the sample row, did experience Al input and so this depletion cannot be extremely effective. Secondly, also because of its position in the row, the Lu sample has developed a significant amount of garnet at the lower surface and this is causing an additional mass gain/change to be recorded. The true behaviour of the upper face might then be much closer to Yb. Thirdly, we do not have a phase diagram for the Lu_2O_3–Al_2O_3–SiO_2 system. Lu has a still smaller ionic radius and for this reason the system should have an even stronger tendency to have a silica-rich liquid in equilibrium with disilicate and garnet at 1500 °C. For reasons of mass conservation the amount of melt formed along with garnet should be less than in the Yb system and this could also help in a fast closure of a protective layer.

We assume that each of these points makes some contribution and hence at this time we cannot distinguish the systems in terms of their protection development kinetics. In particular the time at which a significant protection is obtained in the Lu material is obscured by a continuing Al uptake: the "upper face" values of Fig. 5b misleadingly suggest early and effective protection.

The samples with solid solutions of Y and Yb or Lu behave similar to the Y-sample (Fig. 5a), implying that the garnet found on them is a product of crystallisation during cooling. The presence of melt on the sample surface and inside pores during the corrosion could help in the sintering/recrystallisation of the samples, which would explain the well faceted large crystals of monosilicate (Fig. 3a). It would also provide an explanation for the tendency of the garnet to appear at triple junctions at shorter oxidation times (Fig. 2a and b), as a poorly wetting liquid would prefer to sit there.

It is interesting to note the similarity in the slopes of Fig. 5a for sample Y and all mixed disilicate compositions: the variation is in the narrow range between 1.3×10^{-3} mg cm^{-2} h^{-1} and 2×10^{-3} mg cm^{-2} h^{-1}. As a conclusion, the materials (respectively the melts developed on these on Al ingress) should have a similar silica activity and therefore similar loss kinetics.

If the coverage with melt develops over the time (as might be judged from Figs. 2a–c) and nonetheless we do have a single linear approximation in the loss plot (Fig. 5a), there should also be only minor differences between the loss rate of the disilicate and the one of the melt formed at high temperature.

Alternatively, if a closed melt cover on the samples would be established at $t < 20$ h, higher $a(SiO_2)$ of uncovered disilicate compared to melt-covered portions of the sample might contribute to the observed raised loss rates in the initial phase of the corrosion process.The factor for the alumina input from the gas phase with time is neglected in the rates discussed above and absolute silica loss rates of the samples must accordingly be higher than the measured weight loss rates. Unfortunately, the amount of Al ingress cannot be quantified.

Nonetheless, it is instructive to compare our values to those of other investigations. Following the approach of Opila[9] it should be possible to do this using the relation

$$k_l \propto \frac{P^2}{\sqrt{P_{\text{total}}}}\sqrt{v} \tag{3}$$

with k_l is the linear corrosion rate, P_{H_2O} the water partial pressure, P_{total} the total pressure in the furnace tube and v is the gas velocity.

The results for our conditions from Fig. 5a and the converted values from the literature[3,4,12,18,20,9]) are listed in Table 3.

In discussing the data of Table 3 it should be noted that there are several rather coarse crude assumptions in the conversion by Eq. (3), namely the temperature independence of the $Si(OH)_4$-pressure over silica or the constant boundary layer concentration. Small discrepancies might therefore be attributed to uncertainties from these assumptions.

Table 3
Corrosion rates in mg cm^{-2} h^{-1} from this work and literature

	This work[a]	Lee[b]	Klemm[c]	Yuri[d]	Ueno	Opila
Tube material	Alumina	Alumina	SiC	SiC	Alumina	Fused Quartz
$Y_2Si_2O_7$	-1.92×10^{-3}		-0.15×10^{-3}			
$(Y,Yb)/(Y,Lu)_2Si_2O_7$	-1.3 to -1.9×10^{-3}					
$Yb_2Si_2O_7$	Not linear	-1.5×10^{-3}	-0.15×10^{-3}		-2.3×10^{0}	
$Lu_2Si_2O_7$	Not linear			-1×10^{-3}	-12.7×10^{-3}	
SiO_2	-12.7×10^{-3}					-1.3×10^{-3}

[a] Values from Fig. 5a, i.e. losses related to upper face surface.
[b] From the linearly behaving parts of the samples of Fig. 3.
[c] Conversion from 1450 °C to 1500 °C with data for the temperature dependence of Lu disilicate corrosion from.[12]
[d] Some silica in the original disilicate material suspected.[12]

Table 3 shows very large discrepancies. In the pure Y system there is one order of magnitude difference between our values and those of Klemm.[4] As in our data set the values are masked by an continuing Al uptake, true silica loss rates must be higher still. Klemm performed his experiments in a SiC tube, which will oxidise under those conditions and accordingly should provide a pressure of $Si(OH)_4$ in the reaction gas. It seems likely that this caused a saturation effect, which resulted in a lowered corrosion rate.

The value quoted for Lee[3] for $Yb_2Si_2O_7$ needs some comment. There were two samples of $Yb_2Si_2O_7$ in his experiments. Only one behaved linearly over the 100 h test. The second sample was clearly non-linear, but the run time was too short to decide, whether it would behave asymptotic. We have extracted the linear rate constant from the periods, which could be approximated reasonably. A similar rate constant would be extracted from Fig. 5b of our data. The major difference with the value of Klemm[4] could again be caused by a saturation effect.

The three orders of magnitude difference in comparison of our data with the data of Ueno[18,20] probably reflects another experimental problem: the authors placed their samples on Al_2O_3 plates during the corrosion tests. A reaction of these plates with the samples (including strong melt formation) seems unavoidable and might have caused the high mass losses. The authors of[18,20] do not report Al incorporation in their samples, but an XRD pattern of corroded Lu disilicate[18] shows clear evidence for the formation of a Lu–Al garnet phase during corrosion.

The $Lu_2Si_2O_7$ results are likewise incompatible. Our data suggest an early protective kinetic, while the data of Yuri[12] and Ueno[18,20] indicate linear kinetics with strongly differing rates. Again the high values of Ueno could be due to the placement on alumina holders. Those of Yuri come from experiments in SiC tubes. Here no protection can arise, hence linear kinetics are expected. Due to $Si(OH)_4$ saturation, the value should be on the low side in this case. The high value reported would argue against a better protection against hydro corrosion by $Lu_2Si_2O_7$. However, high rates may also be due to some free SiO_2, which the authors reported to be present in uncorroded Lu disilicate samples.

A serious discrepancy exists in the comparison between the SiO_2-data of our work and that of Opila.[9] Our data indicate values which are higher by an order of magnitude. The minor alumina contamination detected on our silica samples probably caused melt formation. However, its composition should be that of the metastable eutectic in the system alumina–silica, which is at a level of approximately 90% SiO_2.[32] The silica content of the melts in the rare earth oxide systems (Fig. 6) are between about 25 wt% and 40 wt% silica. A factor 2–4 difference in silica activities therefore seems reasonable, so our data are roughly self-consistent and would only point to limited non-ideal behaviour of an alumosilicate melt, increasing the corrosion rate further.

The discrepancy with the data from Opila[9] may also come from some saturation in $Si(OH)_4$ caused by the quartz tube used in her experiments, despite the efforts to limit it.

5. Conclusions

The corrosion of disilicates by water vapor at high temperatures is influenced by alumina containing objects in the gas stream, leading to alumina transfer. In $Y_2Si_2O_7$ and a number of solid solutions with Lu or Yb up to 50% the alumina input causes the formation of a melt. Whether this is accompanied by the formation of oxyapatite or monosilicate depends on the level on impurities, particularly Ca. On cooling the melt crystallizes and yields rare earth garnets.

For those systems the melt ± silicate formation does not create a protective effect. The corrosion is linear, the rates are lower than for pure silica, but only at a level, which is corresponding to their dilution in silica activity (by a factor of 2–5). This has been expected for the pure system[10] and is confirmed here for the Al-bearing system.

Porosity with its accompanied extended surface area causes fast initial mass losses. The formation of secondary phases inside the material causes internal stresses, which can induce crack formation. Strain due to expansion mismatch should act into the same direction during cycling.

We therefore we do not believe that a disilicate layer in those systems has the potential to establish an effective environmental barrier for non-oxide systems.

For Yb and Lu silicates there are indications for the formation of a rare earth garnet layer at high temperature, which has protective power. This yields a logarithmic law for the corrosion: for extended times the mass loss drops asymptotically. Under the assumption that the garnet formation also removes the sink for external alumina, the protection may even become perfect.

To evaluate the potential of this concept further, investigations on oxide film adherence and the control of layer growth are necessary.

References

1. Bondar, I. A. and Galakhov, F. Y., System Al_2O_3–Y_2O_3–SiO_2. *Bull. Acad. Sci. USSR, Div. Chem. Sci. (Engl. Transl.)*, 1964, **7**, 1231–1232.
2. Fabrichnaya, O., Seifert, H. J., Weiland, R., Ludwig, T., Aldinger, F. and Navrotsky, A., Phase equilibria and thermodynamics in the Y_2O_3–Al_2O_3–SiO_2 system. *Z. Metallkd.*, 2001, **92**(9), 1083–1097.
3. Lee, K. N., Fox, D. S. and Bansal, N. P., Rare earth silicate environmental barrier coatings for SiC/SiC composites and Si_3N_4 ceramics. *J. Eur. Ceram. Soc.*, 2005, **25**, 1705–1715.
4. Klemm, H., Fritsch, M. and Schenk, B., Corrosion of ceramic materials in hot gas environment, Ceram. Eng. Sci. Proc. **25** (4) 463–468.
5. Murakami, Y. and Yamamoto, H., Phase equilibria and properties of glasses in the Al_2O_3–Yb_2O_3–SiO_2 system. *J. Ceram. Soc. Jpn.*, 1993, **101**(10), 1101–1106.
6. Klemm, H., Corrosion of silicon nitride materials in gas turbine environment. *J. Eur. Ceram. Soc.*, 2002, **22**, 2735–2740.
7. Jayaseelan, D. D., Ueno, S. and Kanzaki, S., Sol–gel synthesis and coating of nanocrystalline $Lu_2Si_2O_7$ on Si_3N_4 substrate. *Mater. Chem. Phys.*, 2004, **84**, 192–195.
8. Fox, D. S., Opila, E. J., Nguyen, Q. N., Humphrey, D. L. and Lewton, S. M., Paralinear oxidation of silicon nitride in a water-vapor/oxygen environment. *J. Am. Ceram. Soc.*, 2003, **86**(8), 1256–1261.
9. Opila, E. J. and Hann Jr., R. E., Paralinear oxidation of CVD SiC in water vapor. *J. Am. Ceram. Soc.*, 1997, **80**(1), 197–205.

10. Opila, E. J., Robinson, R. C., Fox, D. S., Wenglarz, R. A. and Ferber, M. K., Additive effects on Si_3N_4 oxidation/volatilization in water vapor. *J. Am. Ceram. Soc.*, 2003, **86**(8), 1262–1271.
11. Yuri, I. and Hisamatsu, T. Recession rate prediction for ceramic materials in combustion gas flow. in ASME TURBO EXPO 2003. GT2003-38886, 10 pp.
12. Yuri, I., Hisamatsu, T., Ueno, S. and Ohji, T. Exposure test results of $Lu_2Si_2O_7$ in combustion gas flow at high temperature and high speed. in ASME Turbo Expo 2004. 2004. GT2004-54277, 6 pp.
13. Aparacio, M. and Durán, A., Yttrium silicate coatings for oxidation protection of carbon-silicon carbide composites. *J. Am. Ceram. Soc.*, 2000, **83**(6), 1351–1355.
14. Lee, S. K. and Readey, M. J., Development of a self-forming ytterbium silicate skin on silicon nitride by controlled oxidation. *J. Am. Ceram. Soc.*, 2002, **85**(6), 1435–1440.
15. Weidenmann, K.A., Oxidationsverhalten flüssigphasenverdichteter Nichtoxidkeramiken an feuchter Atmosphäre, in Institut f. Nichtmetallische Anorganische Materialien. 2003. Diploma Thesis, Universität Stuttgart, Stuttgart, p. 97.
16. Eaton, H. E. and Linsey, G. D., Accelerated oxidation of SiC CMC's by water vapor and protection via environmental barrier coating approach. *J. Eur. Ceram. Soc.*, 2002, **22**, 2741–2747.
17. Ueno, S., Jayaseelan, D. D., Ohji, T., Kondo, N. and Kanzaki, S., Preparation and the hydro thermal corrosion resistance of silicon nitride with a Lu-Si-O EBC layer at high temperature. *J. Ceram. Process. Res.*, 2003, **4**(4), 214–216.
18. Ueno, S., Kondo, N., Jayaseelan, D.D., Ohji, T. and Kanzaki, S. High temperature hydro corrosion resistance of silica based oxide ceramics. in ASME TURBO EXPO 2003. 2003. GT2003-38878, 8 pp.
19. Ueno, S., Jayaseelan, D. D., Ohji, T., Kondo, N. and Kanzaki, S., Comparison of water vapor corrosion mechanisms of polycrystalline and eutectic $Lu_2Si_2O_7$. *J. Ceram. Process. Res.*, 2004, **5**(2), 153–156.
20. Ueno, S., Doni Jayaseelan, D. and Ohji, T., Development of oxide-based EBC for silicon nitride. *Int. J. Appl. Ceram. Technol.*, 2004, **1**(4), 362–373.
21. Maier, N., Synthese von Seltenerd-Sisilikaten und deren Korrosionsverhalten an strömender feuchter Atmosphäre, Diploma Thesis, Applied Mineralogy. 2005. University Tuebingen, Tuebingen, 257 pp.
22. Maier, N., Rixecker, G. and Nickel, K. G., Formation and stability of Gd, Y, Yb and Lu disilicates and their solid solutions. *J. Solid State Chem.*, 2006, **179**, 1630–1635.
23. Opila, E. J. and Myers, D. L., Alumina volatility in water vapor at elevated temperatures. *J Am Ceram Soc*, 2004, **87**(9), 1701–1705.
24. Opila, E. J., Oxidation kinetics of chemically vapor-deposited silicon carbide in wet oxygen. *J. Am. Ceram. Soc.*, 1994, **77**(3), 730–736.
25. Opila, E. J., Oxidation and volatilization of silica formers in water vapor. *J. Am. Ceram. Soc.*, 2003, **86**(8), 1238–1248.
26. Cinibulk, M. K. and Thomas, G., Fabrication and secondary phase crystallization of rare-earth disilicate-silicon nitride ceramics. *J. Am. Ceram. Soc.*, 1992, **75**(8), 2037–2043.
27. Cinibulk, M. K., Thomas, G. and Johnson, S. M., Oxidation behavior of rare-earth disilicate silicon nitride ceramics. *J. Am. Ceram. Soc.*, 1992, **75**(8), 2044–2049.
28. Kolitsch, U., Seifert, H. J. and Aldinger, F., Phase relationships in the systems RE_2O_3–Al_2O_3–SiO_2 (RE = rare earth element, Y, and Sc). *J. Phase Equilibr.*, 1998, **19**(5), 426–433.
29. Nickel, K. G. and Gogotsi, Y. G., Corrosion of hard materials. In *Handbook of ceramic hard materials*, ed. R. Riedel. VCH–Wiley, Weinheim, 2000, pp. 140–182.
30. Barlier, P. and Torre, J. P., Improvement of the oxidation behavior of reaction bonded silicon nitride by addition of aluminium. *Mater. Sci. Mon.*, 1980, **6**, 718–728.
31. Porz, F. and Thümmler, F., Oxidation mechanism of porous silicon nitride. *J. Mater. Sci.*, 1984, **19**, 1283–1295.
32. Aksay, I. A. and Pask, J. A., Stable and metastable equilibria in the system SiO_2–Al_2O_3. *J. Am. Ceram. Soc.*, 1975, **58**(11/12), 507–512.